NASA/CR—2004-212917 AIAA–2004–0062

An Evaluation of Jet Impingement Heat Transfer Correlations for Piccolo Tube Application

William B. Wright
QSS Group, Inc., Cleveland, Ohio

April 2004

The NASA STI Program Office . . . in Profile

Since its founding, NASA has been dedicated to the advancement of aeronautics and space science. The NASA Scientific and Technical Information (STI) Program Office plays a key part in helping NASA maintain this important role.

The NASA STI Program Office is operated by Langley Research Center, the Lead Center for NASA's scientific and technical information. The NASA STI Program Office provides access to the NASA STI Database, the largest collection of aeronautical and space science STI in the world. The Program Office is also NASA's institutional mechanism for disseminating the results of its research and development activities. These results are published by NASA in the NASA STI Report Series, which includes the following report types:

- TECHNICAL PUBLICATION. Reports of completed research or a major significant phase of research that present the results of NASA programs and include extensive data or theoretical analysis. Includes compilations of significant scientific and technical data and information deemed to be of continuing reference value. NASA's counterpart of peer-reviewed formal professional papers but has less stringent limitations on manuscript length and extent of graphic presentations.

- TECHNICAL MEMORANDUM. Scientific and technical findings that are preliminary or of specialized interest, e.g., quick release reports, working papers, and bibliographies that contain minimal annotation. Does not contain extensive analysis.

- CONTRACTOR REPORT. Scientific and technical findings by NASA-sponsored contractors and grantees.

- CONFERENCE PUBLICATION. Collected papers from scientific and technical conferences, symposia, seminars, or other meetings sponsored or cosponsored by NASA.

- SPECIAL PUBLICATION. Scientific, technical, or historical information from NASA programs, projects, and missions, often concerned with subjects having substantial public interest.

- TECHNICAL TRANSLATION. English-language translations of foreign scientific and technical material pertinent to NASA's mission.

Specialized services that complement the STI Program Office's diverse offerings include creating custom thesauri, building customized databases, organizing and publishing research results . . . even providing videos.

For more information about the NASA STI Program Office, see the following:

- Access the NASA STI Program Home Page at ***http://www.sti.nasa.gov***

- E-mail your question via the Internet to help@sti.nasa.gov

- Fax your question to the NASA Access Help Desk at 301–621–0134

- Telephone the NASA Access Help Desk at 301–621–0390

- Write to:
  NASA Access Help Desk
  NASA Center for AeroSpace Information
  7121 Standard Drive
  Hanover, MD 21076

NASA/CR—2004-212917 AIAA–2004–0062

An Evaluation of Jet Impingement Heat Transfer Correlations for Piccolo Tube Application

William B. Wright
QSS Group, Inc., Cleveland, Ohio

Prepared for the
42nd Aerospace Sciences Meeting and Exhibit
sponsored by the American Institute of Aeronautics and Astronautics
Reno, Nevada, January 5–8, 2004

Prepared under Grant NAG3–00145

National Aeronautics and
Space Administration

Glenn Research Center

April 2004

Acknowledgments

The author would like to acknowledge Derek Rounds, Cessna Aircraft Company, Sam Lee, QSS Group, Inc., Gene Addy, NASA Glenn Research Center, and Andy Broeren, University of Illinois at Urbana-Champaign, for access to data from their test in a very short time period and for help with data reduction. The author would like to thank Colin Bidwell for assistance with using TECPLOT. The author would also like to thank NASA Glenn Research Center for the continued financial support of this contract.

Available from

NASA Center for Aerospace Information
7121 Standard Drive
Hanover, MD 21076

National Technical Information Service
5285 Port Royal Road
Springfield, VA 22100

Available electronically at http://gltrs.grc.nasa.gov

AN EVALUATION OF JET IMPINGEMENT HEAT TRANSFER CORRELATIONS FOR PICCOLO TUBE APPLICATION

William B. Wright
QSS Group, Inc.
Cleveland, Ohio 44135

ABSTRACT

Impinging jets have been used for a wide variety of applications where high rates of heat transfer are desired. This report will present a review of heat transfer correlations that have been published. The correlations were then added to the LEWICE software to evaluate the applicability of these correlations to a piccolo tube anti-icing system. The results of this analysis were then compared quantitatively to test results on a representative piccolo tube system.

NOMENCLATURE

A	Area ratio (dimensionless)
c	chord (m)
c_n	spanwise distance between holes (m)
c_x	chordwise distance between holes (m)
C_p	heat capacity (kJ/kgK)
d	jet hole diameter (m)
D	diameter of semi-cylinder (m)
G	mass flux (kg/m^2s)
h	Heat transfer coefficient (kW/m^2K)
k	Thermal conductivity (kW/mK)
$\dot{m}$	Mass flow rate per unit span (kg/ms)
N_r	Number of jet rows
Nu	Nusselt number $= \frac{hd}{k_a}$
$\overline{Nu}$	average Nusselt number
q"	Heat flux (kW/m^2)
Pr	Prandtl number $= \frac{C_p \mu_a}{k_a}$
r	radial distance from hole (m)
Re	Reynolds number $= \frac{Gd}{\mu_a}$
s	wrap distance (m)
T	Temperature (K)
w	slot width (m)
z_n	distance from hole to wall (m)

Correlation Constants

a, B, b, C, c, c_o, m, n, n_x, n_y, n_z

Greek Letters

α	impingement angle (degrees)
μ	viscosity (kg/m-s)
ρ	density (kg/m^3)

Subscripts

a	air
c	crossflow
j	jet
max	maximum value
o	stagnation
q	heat flux

INTRODUCTION

The removal and/or prevention of ice on aircraft components is vital to aircraft performance and operation. Even small amounts of ice can have disastrous consequences. Because of this, several methods of ice prevention and removal have been designed. Methods of ice control can be arranged into two broad categories: anti-icing methods and de-icing methods. Anti-icing methods are concerned with the prevention or minimization of ice buildup on protected surfaces. De-icing methods are concerned with ice removal after and during ice build up.

The primary means of preventing ice formation on wings and engine inlets for modern commercial transport aircraft is by extracting hot air from the compressor and blowing it on the inside surface of the leading edge through small holes drilled in a pipe. Ice accretion is prevented by supplying enough energy to evaporate the impinging water (evaporative anti-icing) or by maintaining a surface temperature above freezing (running wet anti-icing). This report will demonstrate that the amount of heat supplied can be calculated by correlations based upon hole and pipe diameter, the number of holes, the mass flow rate of the air and the supply temperature.

Impinging jets are a widely used method for heating and cooling applications. Martin[1] and later Jambunathan et al.[2] provide a thorough review of heat

transfer data from impinging jets. Most of the research referenced in these works was performed using a single jet or a group of jets impinging on a flat plate. Correlations were presented in these reports for the average Nusselt number. While this information is useful, piccolo tubes impinge on the curved inside surface of a wing or inlet. Additionally, the effect of jet interaction, jet angle, and Nusselt number distribution are also of interest.

Livingood and Gauntner[3] were the first to look at a row of jets impinging on a concave surface for a turbine cooling application. Similar studies were performed by Hollworth and Berry[4] and also Hrycak.[5] These reports included the first attempts at creating correlations for average Nusselt number.

Gau and Chung[6] reported on the effects of both concave and convex surfaces and included results from slots as well as orifices. Sparrow and Lovell[7] studied the effects of jet impingement at oblique angles. Tawfek[8] expanded this analysis for a wider range of impingement angles and Reynolds numbers. Wu et al.[9] performed a numerical study of different impingement angles using 3D Naviér-Stokes. Goldstein and Sol[10] looked at the effect of entrainment on heat transfer that can occur near the leading edge. Goldstein et al.[11] used a similar technique to examine variation of recovery factor. Florshuetz et al.[12] studied the spanwise effects and the effect of staggered jet arrays versus inline arrays.

Recently, experimental techniques have advanced that allow accurate measurement and correlation of local Nusselt number. Campbell et al.[13] and Crafton et al.[14] presented a methodology using temperature sensitive paint to obtain more accurate and more detailed measurements of heat transfer at different angles. Ichimiya[15] performed a similar study using a thermosensitive liquid crystal. Maurel and Solliec[16] used laser Doppler velocimetry and particle image velocimetry to measure details of the jet flow field as well as heat transfer. Tawfek[17] used heat flux sensors to obtain local and average heat transfer measurements. He also obtained local pressure distributions using a Perspex disk. Huber and Viskanta[18] used the liquid crystal technique to examine the effect of jet spacing. Huang and El-Genk[19] used a heated plate to take measurements of local and average heat transfer. Brown et al.[20] used thermocouple measurements for a piccolo tube system but did not publish the coefficients of the correlation obtained. However, the form of their correlation is similar to the other reports which suggest that the other correlations may be useful.

The report is divided into three sections. The first section will provide a description of the LEWICE[21] model, with emphasis on the anti-icing physics. The second section will describe the specific correlations tested. The third section will compare the anti-icing results using these correlations with data taken in the Icing Research Tunnel (IRT) on a representative piccolo tube system.

LEWICE

The computer program LEWICE embodies an analytical ice accretion model that evaluates the thermodynamics of the freezing process that occurs when supercooled droplets impinge on a body. The atmospheric parameters of temperature, pressure, and velocity, and the meteorological parameters of liquid water content (LWC), droplet diameter, and relative humidity are specified and used to determine the shape of the ice accretion. The surface of the clean (un-iced) geometry is defined by segments joining a set of discrete body coordinates. The software consists of four major modules. They are 1) the flow field calculation, 2) the particle trajectory and impingement calculation, 3) the thermodynamic and ice growth calculation, and 4) the modification of the current geometry by addition of the ice growth.

LEWICE applies a time-stepping procedure to "grow" the ice accretion. Initially, the flow field and droplet impingement characteristics are determined for the clean geometry. The ice growth rate on each segment defining the surface is then determined by applying the thermodynamic model. When a time increment is specified, this growth rate can be interpreted as an ice thickness and the body coordinates are adjusted to account for the accreted ice. This procedure is repeated, beginning with the calculation of the flow field about the iced geometry, then continued until the desired icing time has been reached.

The thermal module calculates the 2D transient (time-dependant) heat conduction in a body. It can handle multiple composite layers, where each layer can have different thermal properties including temperature dependence and anisotropy. Ice growth can be predicted with or without heat, and the model includes various routines for ice shedding and water runback. It can also function as an ice accretion simulator with heater power turned off. The original deicer program has been documented in previous reports.[21–23]

While this module was originally designed to simulate an electrothermal de-icer, a bleed air system can be analyzed through the use of appropriate boundary conditions. This method, based upon the model of Al-Khalil,[24] requires that the user supply either a heat flux or heat transfer coefficient as a boundary condition. For design purposes, users have indicated a preference for a system that instead inputs piccolo tube design parameters. These parameters include hole diameter, jet distance from the wall and jet spacing. The next section of this report describes empirical equations that have been developed which may be appropriate for anti-icing design.

LEWICE also contains a feature that assumes 1D heat conduction in the normal direction. This assumption states that while the internal flow is 3D and the external flow and water collection are primarily 2D, heat conduction through the surface is primarily 1D. Previously, the user could choose to assume evaporative heating or a constant (above freezing) surface temperature boundary in this mode. The calculation was performed separately from the icing analysis and did not affect the ice shape. It was created for performing quick design analysis of anti-icing systems. This feature has recently been extended for electrothermal and piccolo tube systems. The user can now specify the heat inputs in the same manner as the 2D conduction model. LEWICE will then perform the same type of analysis (except assuming 1D heat transfer), including the calculation of residual ice growth if insufficient heat is added. This mode will allow the user to perform more rapid preliminary design analysis of systems.

PICCOLO TUBE CORRELATIONS

The reports discussed earlier found that local and average Nusselt numbers were primarily functions of the jet Reynolds number, the jet spacing, and the distance to the wall. Effects of curvature and impingement angle were also studied. Some of the reports listed previously only provided a partial correlation. This section will present each of the full correlations found and their range of applicability. As with any correlation, care must be taken when extrapolating outside of the applicable range. Unless otherwise noted, the correlations were developed for arrays of circular holes impinging normally on a flat plate. Additionally, Reynolds number was calculated for circular cross-section holes by using the mass flow rate per unit span:

$$\mathrm{Re} = \frac{4\dot{m}}{\pi N_r \mu}\frac{c_n}{d}$$

Martin[1]

$$\overline{Nu} = \left[1+\left(\frac{z_n/d}{0.6/\sqrt{A}}\right)^6\right]^{-0.05}\sqrt{A}\,\frac{1-2.2\sqrt{A}}{1+0.2(z_n/d-6)\sqrt{A}}\,\mathrm{Re}^{2/3}$$

where A is the dimensionless area

$$A = \frac{\frac{\pi}{4}d^2}{c_n c_x}$$

$2{,}000 \le \mathrm{Re} \le 100{,}000$

$0.004 \le A \le 0.04$

$2 \le z_n/d \le 12$

Hrycak[5]

Flat Plate

$$Nu_o = 0.763\,\mathrm{Pr}^{0.39}\,\mathrm{Re}^{0.5}\left(\frac{z_n}{d}\right)^{0.16}$$

Semi-Cylinder

$$Nu_o = 1.85\,\mathrm{Pr}^{1/3}\,\mathrm{Re}^{0.695}\left(\frac{d}{D_c}\right)^{1.05}$$

$14{,}000 \le \mathrm{Re} \le 67{,}000$

$1.5 \le z_n/d \le 7$

$D_c = 127$ mm

Gau and Chung[6]

Slot impinging on Concave Surface

Re is based on the slot width, w.

$$\overline{Nu} = 0.251\mathrm{Re}^{0.68}\left(\frac{D_c}{w}\right)^{-0.38}\left(\frac{z_n}{w}\right)^{0.15}$$

$$Nu_o = 0.729\mathrm{Re}^{0.5}\left(\frac{D_c}{w}\right)^{-0.14}\left(\frac{z_n}{w}\right)^{0.16}$$

$8 \le Z_n/w \le 16$

$$\overline{Nu} = 0.394\,\mathrm{Re}^{0.68}\left(\frac{D_c}{w}\right)^{-0.38}\left(\frac{z_n}{w}\right)^{-0.32}$$

$$Nu_o = 1.76\mathrm{Re}^{0.54}\left(\frac{D_c}{w}\right)^{-0.15}\left(\frac{z_n}{w}\right)^{-0.38}$$

$6{,}000 \le \mathrm{Re} \le 35{,}000$

$8 \le D_c/w \le 45.7$

$2 \le Z_n/w \le 8$

Tawfek[8]

Angled impingement

S_{max} represents the wrap distance measured from the impingement location where the maximum Nusselt number is located.

$$Nu_o = 0.16\mathrm{Re}^{0.71}\left(\frac{z_n}{d}\right)^{-0.14}\left(\frac{d}{D_c}\right)^{-0.35}$$

$$Nu_{\max} = 0.142\mathrm{Re}^{0.71}\,\alpha^{0.194}\left(\frac{z_n}{d}\right)^{-0.14}\left(\frac{d}{D}\right)^{-0.35}$$

$$\frac{S_{\max}}{d} = \mathrm{Re}^{0.611}\left(\frac{z_n}{d}\right)^{-0.14}\left[0.005-0.0016\alpha-0.0012\alpha^2\right]$$

$3{,}800 \le \mathrm{Re} \le 40{,}000$

$20° \le \alpha \le 90°$

$7 \le z_n/d \le 30$

$0.06 \le d/D_c \le 0.14$

Goldstein and Seol[10]

$$\overline{Nu} = \frac{2.9\,\mathrm{Re}^{0.7}\exp\left(-0.09\left(\frac{s}{d}\right)^{1.4}\right)}{22.8+\left(\frac{c_n}{d}\right)\left(\frac{z_n}{d}\right)^{0.5}}$$

$$10{,}000 \le \mathrm{Re} \le 40{,}000$$
$$2 \le z_n/d \le 8$$
$$4 \le c_n/d \le 8$$
$$0 \le s/d \le 6$$

Goldstein et al.[11]

Nu_q is based on the assumption of constant heat flux whereas Nu is based upon the assumption of constant temperature difference.

$$\overline{Nu} = \mathrm{Re}^{0.76}\frac{24-\left|\left(\frac{z_n}{d}-7.75\right)\right|}{533+44\left(\frac{r}{d}\right)^{1.285}}$$

$$\overline{Nu}_q = \mathrm{Re}^{0.76}\frac{24-\left|\left(\frac{z_n}{d}-7.75\right)\right|}{533+44\left(\frac{r}{d}\right)^{1.394}}$$

$$61{,}000 \le \mathrm{Re} \le 124{,}000$$
$$0.5 \le r/d \le 32$$
$$6 \le z_n/d \le 12$$

The second Goldstein correlation listed above was used in LEWICE for the purpose of demonstrating the correlation's use in the software. Values calculated using this correlation provide the average Nusselt number at each radial position rather than the local Nusselt number. When this process started, it was thought that the high Reynolds numbers of this correlation were necessary for piccolo tube applications. However, the experimental data used for comparison had a Reynolds number below the range of this correlation.

Florschuetz[12]

Jet array with crossflow

$$\overline{Nu} = C\,\mathrm{Pr}^{1/3}\,\mathrm{Re}^{m}\left[1-B\left[\frac{z_n}{d}\frac{G_c}{G_j}\right]^n\right]$$

where C, B m and n fit the general form

$$C,B,m,n = c_o\left(\frac{c_x}{d}\right)^{n_x}\left(\frac{c_n}{d}\right)^{n_y}\left(\frac{z_n}{d}\right)^{n_z}$$

based on the following tables.

Table 1: Coefficients for inline holes

	c_o	n_x	n_y	n_z
C	1.18	-0.944	-0.642	0.169
m	0.612	0.059	0.032	-0.02
B	0.437	-0.095	-0.219	0.275
n	0.092	-0.005	0.599	1.04

Table 2: Coefficients for staggered holes

	c_o	n_x	n_y	n_z
C	1.87	-0.771	-0.999	-0.26
m	0.571	0.028	0.092	0.039
B	1.03	-0.243	-0.307	0.059
n	0.442	0.098	-0.003	0.304

$$2{,}500 \le \mathrm{Re} \le 70{,}000$$
$$5 \le c_x/d \le 15 \text{ (inline)}$$
$$5 \le c_x/d \le 10 \text{ (staggered)}$$
$$4 \le c_n/d \le 8$$
$$1 \le z_n/d \le 3$$

Tawfek[17]

$$\overline{Nu} = 0.453\,\mathrm{Pr}^{1/3}\,\mathrm{Re}^{0.691}\left(\frac{z_n}{d}\right)^{-0.22}\left(\frac{c_n}{d}\right)^{-0.38}$$

$$3{,}400 \le \mathrm{Re} \le 41{,}000$$
$$2 \le c_n/d \le 30$$
$$6 \le z_n/d \le 58$$

Huber and Viskanta[18]

$$\overline{Nu} = 0.285\,\mathrm{Re}^{0.71}\,\mathrm{Pr}^{1/3}\left(\frac{z_n}{d}\right)^{-0.123}\left(\frac{c_n}{d}\right)^{-0.725}$$

$$3{,}400 \le \mathrm{Re} \le 20{,}500$$
$$0.25 \le z_n/d \le 6$$
$$4 \le c_n/d \le 8$$

Huang and El-Genk[19]

$$\overline{Nu} = \mathrm{Re}^{0.76}\,\mathrm{Pr}^{0.42}\left[a+b\left(\frac{z_n}{d}\right)+c\left(\frac{z_n}{d}\right)^2\right]$$

where

$$a = 10^{-4}\left[506+13.3\left(\frac{r}{d}\right)-19.6\left(\frac{r}{d}\right)^2+2.41\left(\frac{r}{d}\right)^3-0.0904\left(\frac{r}{d}\right)^4\right]$$

$$b = 10^{-4}\left[32-24.3\left(\frac{r}{d}\right)+6.53\left(\frac{r}{d}\right)^2-0.694\left(\frac{r}{d}\right)^3+0.0257\left(\frac{r}{d}\right)^4\right]$$

$$c = -3.85*10^{-4}\left[1.147+\left(\frac{r}{d}\right)\right]^{-0.0904}$$

$$6{,}000 \le \mathrm{Re} \le 60{,}000$$
$$0 \le r/d \le 10$$
$$1 \le z_n/d \le 12$$

BLEED AIR RESULTS

The model used for comparison in this report is shown in Figure 1. A two week entry was performed in the Icing Research Tunnel (IRT) in Sept. 2003 by Lee, Addy and Broeren[25] for the purpose of documenting residual ice shapes from a piccolo tube system. It is not the intent of the paper to report on the full findings of that test entry. This report will only present preliminary thermal data for comparison with the correlation model.

Figure 1: Piccolo Tube Test Model

The model had an average chord length of 1.52 m with a slight 8° sweep. The airfoil profile is similar to the NACA 23014 model used in previous IRT entries as shown in Figure 2. Thermocouples were placed at two different spanwise sections on the inside surface of the airfoil at the locations. A schematic of the thermocouple locations relative to the hole locations is shown in Figure 3.

Figure 2: Profile of Airfoil Used in Comparison

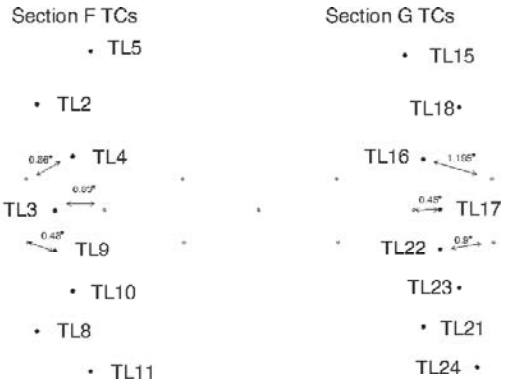

Figure 3: Thermocouple Locations on Piccolo Tube Model

In Figure 3 above, the spanwise direction is horizontal while the leading edge has been unwrapped to show the thermocouple locations. The locations where the jets impinge the surface are shown as open circles. The holes are 1.32 mm in diameter and the distance between holes is 6.6 cm or 50 hole diameters. In the comparisons below, one complete set of jets spanwise was simulated. The center row of holes resides on the airfoil leading edge and in the comparisons will be referred to as Jet 1. The lower surface jet row was labeled Jet 2 and the upper surface jet row was labeled Jet 3.

The spanwise distance between the two rows of thermocouples is greater than that shown in the diagram above, although the relative distance from a thermocouple to a hole is correctly displayed. The diagram was presented in this fashion so that both instrumentation rows could be shown. The thermocouple locations were selected such that the piccolo flow did not impinge directly. The thermocouple coordinates relative to the impingement location of the leading edge hole is shown in Table 3.

Table 3: Thermocouple Locations

TC #	x(m)	y(m)	z(m)
TL5	0.0483	-0.0390	-0.0058
TL15	0.0467	-0.0385	-0.0038
TL2	0.0272	-0.0316	-0.0287
TL18	0.0259	-0.0311	0.0193
TL4	0.0083	-0.0200	-0.0135
TL16	0.0075	-0.0191	0.0041
TL17	0.0000	0.0005	0.0112
TL3	0.0000	0.0008	-0.0211
TL22	0.0033	0.0169	0.0112
TL9	0.0035	0.0175	-0.0211
TL23	0.0105	0.0318	0.0193
TL10	0.0112	0.0330	-0.0135
TL24	0.0204	0.0453	0.0041
TL8	0.0216	0.0467	-0.0287
TL21	0.0321	0.0576	0.0269
TL11	0.0336	0.0588	-0.0058

The de-icing system also contained an inner liner to increase the heat transfer downstream of the tube. A cross-section view of the airfoil with this liner is shown in Figure 4. In LEWICE, the liner was modeled by increasing the flow velocity using the Bernoulli equation. The increased velocity was used in the correlation to get the heat transfer in this region. It should be noted that even if the Bernoulli assumption is correct, the modeling of the liner in this manner is wrong, since the correlation was developed for impinging jets and not for crossflow situations.

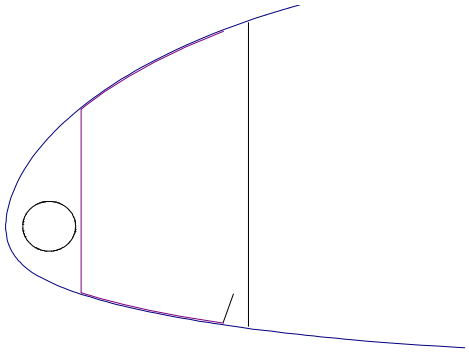

Figure 4: Cross-section of Piccolo tube with Liner

Two cases from the IRT entry were selected to demonstrate the capabilities of the correlation. A warm temperature condition and a cold temperature condition with the same bleed air flow rate were selected from the test matrix. The conditions are shown in Table 4. The mass flow rate given for these conditions represented typical values for this test.

Table 4: Test Conditions

	Case 1	Case2
T_o (°F)	23.1	-19.1
V (kts)	115	110
MVD	29	29
LWC	0.87	0.67
AOA	3	3
time (min)	22.5	8.6
m_{air} (lb/ft-s)	0.01	0.01
T_{air} (°F)	350	350

Using the mass flow rate and the piccolo tube geometry, values that can be input into the various correlations can be calculated. Table 5 summarizes these inputs. The values in this table were used in the Goldstein[11] correlation to calculate Nusselt number. The heat transfer coefficients from this calculation are shown in Figure 5 at three spanwise values: over the centerline of Jet 1, over the centerline of Jets 2 and 3, and at the span location between the jets. The maximum heat transfer coefficient calculated was just over 1 kW/m^{2}K (176 BTU/ft^{2}hr°F) and decreases rapidly away from the jet centerline. In the region between jets, the maximum heat transfer coefficient was under 0.3kW/m^{2}K which demonstrates that significant cooling occurs spanwise. The heat transfer was increased in the liner region as shown by the jump in the curves.

Table 5: Piccolo Inputs for Correlations

Re	11870
z_n/d (Jet 1)	6.9
z_n/d (Jet 2)	5.8
z_n/d (Jet 3)	8.1
c_n/d	50

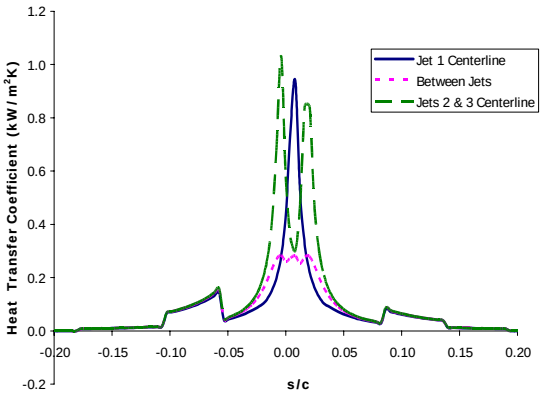

Figure 5: Heat Transfer Coefficients at Selected Spanwise Locations

Calculations of surface temperature were then performed at each of the spanwise locations where a thermocouple measurement was recorded. Several other spanwise locations, ranging from the centerline of Jet 1 to the centerline of Jets 2 and 3, were also calculated to determine the maximum surface temperature and to estimate the temperature gradient. A total of 100 spanwise cases were calculated for each condition. Figure 6 shows the temperature distribution at the three spanwise locations where the heat transfer coefficients were plotted.

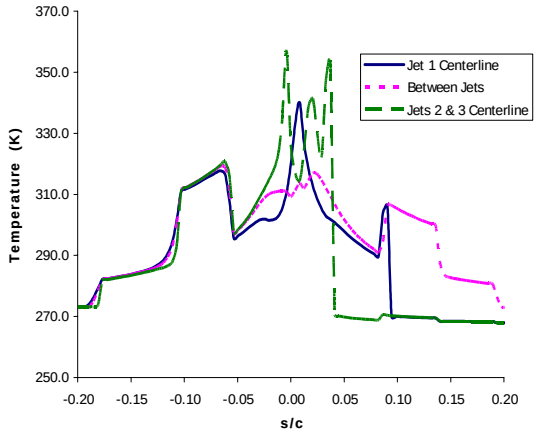

Figure 6: Temperature Variation for Case1

The limitations of the 1D conduction approximation are apparent in this figure. For example, the surface temperature for the Jet 1 centerline location drops over 90°C (from over 350 K to 270 K) as soon as the simulation evaporates all of runback water. The increase in surface temperature over the liner is considered to be an artifact of the model. The calculated temperature gradients in both the chordwise and spanwise directions appear larger than expected.

The spanwise variation in temperature also creates a difference in the calculated residual ice shape, shown in Figure 7.

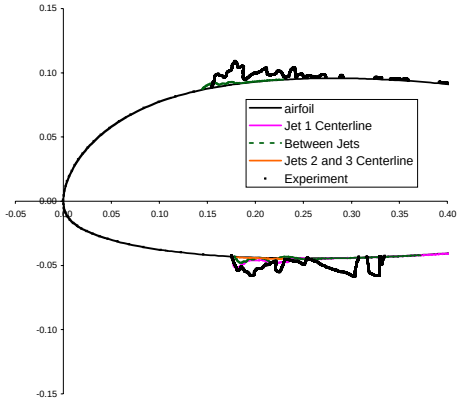

Figure 7: Residual Ice Shape for Case1

The ridge ice location is predicted well by the model, however the mass of residual ice is underpredicted. There are several factors that could have caused this result. Primarily, the piccolo heat transfer coefficient could be overpredicted by the correlation. Additionally, it is acknowledged that the increased heat transfer from the liner would not be modeled by these correlations.

The results from each of the 100 spanwise cuts can be merged into a single file for display purposes. The results of this process, taking advantage of the periodic spanwise boundary condition, is shown in Figures 8 and 9.

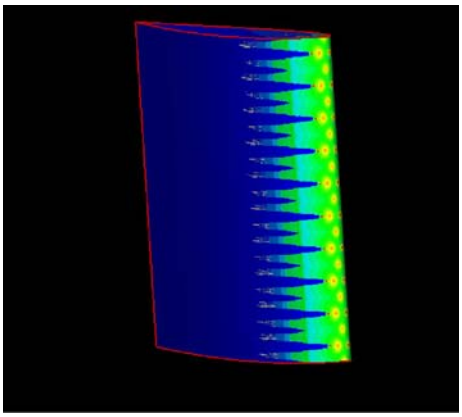

Figure 8: Upper Surface Ice for Case1

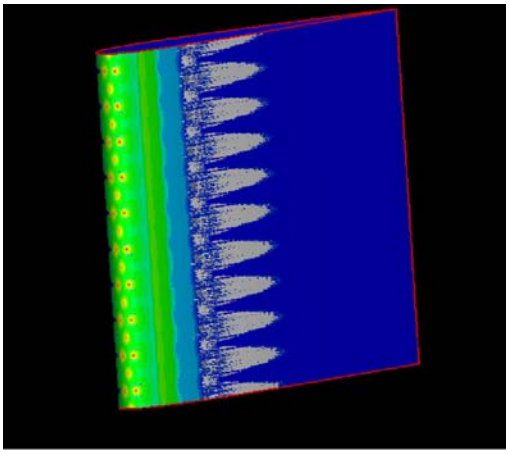

Figure 9: Lower Surface Ice for Case1

Finally, the predicted temperatures at each thermocouple can be extracted from the individual runs and plotted against the experimental data. This result is shown in Figure 10. In this plot, the temperatures are plotted solely as a function of wrap distance even though all of the thermocouples are not at the same spanwise locations. The results show that LEWICE predicts higher temperatures than the experimental data. This result is consistent with the residual ice shape result. Higher surface temperatures will lead to higher amounts of evaporation and a smaller runback shape. It is estimated that the correlation would need to be 20% lower in order to match the experimental temperature profile.

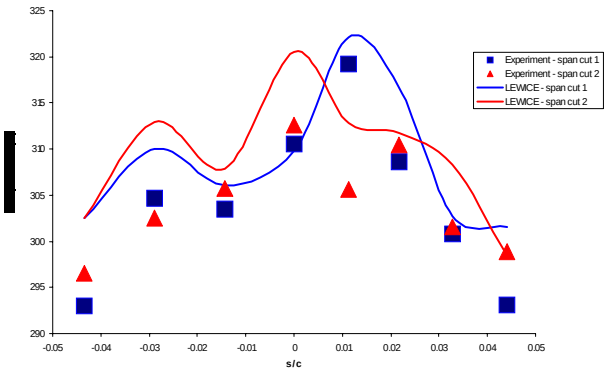

Figure 10: Temperature Comparison for Case1

The same factors that affected the first case can also be seen in the results from Case 2. Figure 11 shows the surface temperature distribution for this condition. This case shows a larger variation in surface temperature due to the liner. This result suggests that the effects of the liner were overpredicted by this model.

The differences and percent differences were calculated by the following equations:

$$abs.diff = |T_{\exp} - T_{LEWICE}|$$

$$\%diff = \frac{|T_{\exp} - T_{LEWICE}|}{T_{\exp,\max} - T_{\infty}}$$

For Case 1, the average temperature difference was 5.1 °C (9.2 °F) or 18% of the maximum temperature rise.

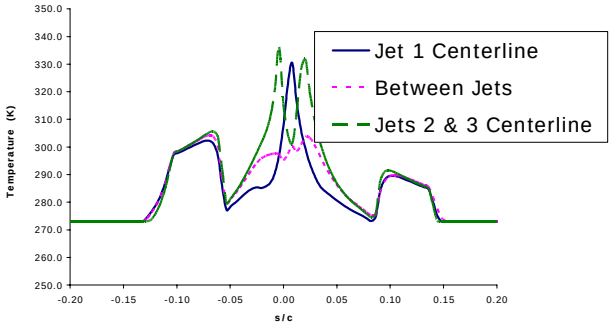

Figure 11: Surface Temperature Distributions for Case 2

This result also shows that the temperature between the jets and the liner is only slightly above freezing. A slightly lower piccolo heat transfer coefficient could result in ice formation at this location. It should also be noted that LEWICE was modified for these runs such that the external boundary layer was kept laminar over the heated region. If this assumption does not hold, a higher external heat transfer coefficient can result. These factors help to explain the residual ice shape prediction in Figure 12.

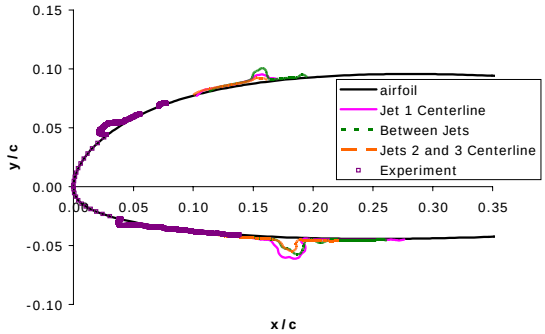

Figure 12: Residual Ice Shape for Case 2

In this case, LEWICE predicts an aerodynamically severe ice ridge similar to but larger than the experimental ice shape. LEWICE places the ice ridge behind the liner boundary rather than in front as shown by the experimental data. This result shows that an improved model for the liner can result in more accurate predictions. The spanwise cuts were again merged to produce a pseudo-3D view of the LEWICE results. The upper and lower surface ice accretions are shown in Figures 13 and 14, respectively.

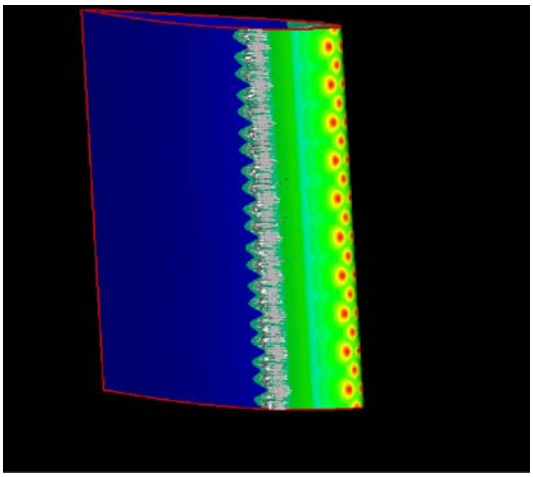

Figure 13: Upper Surface Ice for Case2

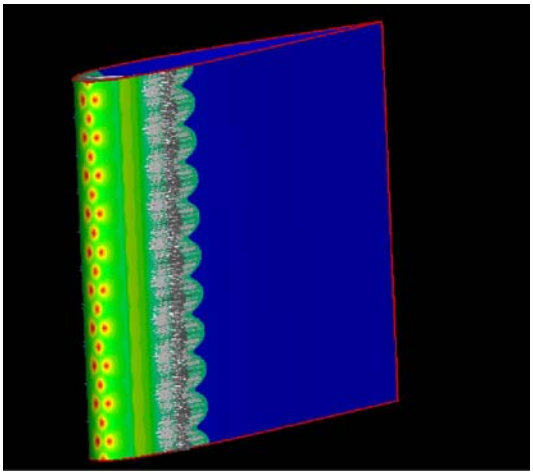

Figure 14: Lower Surface Ice for Case2

The predicted temperatures at each thermocouple location were again extracted from the individual runs and plotted in Figure 15. In this case, the LEWICE predictions appear to be closer to the measured experimental data. As such, the amount of residual ice is closer to the experimental data. However, since the model used for the liner increased temperatures downstream, the ice did not form until after the runback water had passed the liner.

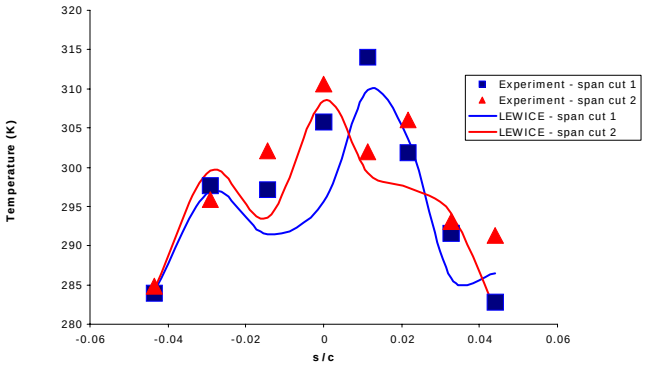

Figure 15: Temperature Comparison for Case 2

In this case, the average temperature difference was 4.3°C (7.8°F) while the percentage difference was 10.5%. This percentage is much lower due to the larger denominator used.

CONCLUSIONS

A literature search was performed which yielded several candidate correlations that could be applicable to piccolo tube anti-icing. Representative values for heat transfer coefficient were calculated from one such correlation and applied to a piccolo tube system for which temperature data exists. Surface temperatures and residual ice shape were compared to the experimental test data for two cases. The results showed that the correlation overpredicted surface temperature, which resulted in different ice residual patterns from the experimental shapes. However, the technique shows promise for rapidly obtaining first order estimates of piccolo tube performance. A separate correlation will be needed for handling the inner liner.

REFERENCES

1. Martin, H., "Heat and Mass Transfer Between Impinging Gas Jets and Solid Surfaces," Adv. in Heat Transfer, Vol. 13, pp. 1–60, 1977.
2. Jambunathan, K., Lai, E., Moss, M.A., and Button, B.L., "A Review of Heat Transfer Data for Single Circular Jet Impingement," Int. J. Heat and Fluid Flow, Vol. 13, #2, June 1992.
3. Livingood, J.N.B. and Gauntner, J.W., "Local Heat-Transfer Characteristics of a Row of Circular Air jets Impinging on a Concave Semi-Cylindrical Surface," NACA TM E–7117, 1972.
4. Hollworth, B. R. and Berry, R.D., "Heat Transfer From Arrays of Impinging Jets with Large Jet-to-Jet Spacing," Trans. of the ASME, v. 100, pp. 352–7, May 1978.
5. Hrycak, P., "Heat Transfer From a Row of Impinging Jets to Concave Cylindrical Surfaces," Intl. J. Heat and Mass Trans., Vol. 24, pp. 407–419, 1981.
6. Gau, C. and Chung, C.M., "Surface Curvature Effect on Slot-Air-Jet Impingement Cooling Flow and Heat Transfer Process," Trans. of the ASME, Vol. 113, pp. 858–864, Nov. 1991.
7. Sparrow, E.M. and Lovell, B.J., "Heat Transfer Characteristics of an Oblique Impinging Circular Jet," Tans. of The ASME, Vol. 102, pp. 202–209, May 1980.
8. Tawfek, A.A., "Heat Transfer Studies of the Oblique Impingement of Round Jets upon a Curved Surface," Heat and Mass Trans., Vol. 38, pp. 467–75, 2002.
9. Wu, J., Tang, L., Luke, E.A., and Tong, X., "A Comprehensive Numerical Study of Jet Flow Impingement over Flat Plates at Varied Angles," AIAA–2001–0745, Jan. 2001.
10. Goldstein, R.J. and Sol, W.S., "Heat Transfer to a Row of Impinging Circular Air Jets Including the Effect of Entrainment," Intl. J. of Heat and Mass Trans., Vol. 34, #8, pp. 2133–2147, 1991.
11. Goldstein, R. J., Behbahni, A. I. and Heppelman, K. K., "Streamwise Distribution of the Recovery Factor and the Local Heat Transfer Coefficient to an impinging Circular Air Jet," Intl. J. of Heat and Mass Trans., Vol. 29, #8, pp. 1227-1235, 1986.
12. Florshuetz, L.W., Metzger, D.E., and Truman, C.R., "Jet Array Impingement with Crossflow—Correlation of Streamwise Resolved Flow and Heat Transfer Distributions," NACA CR–3373, Jan. 1981.
13. Campbell, B.T., Crafton, J., Witte, G.R., and Sullivan, J.P., "Laser Spot Heating/Temperature Sensitive Paint Heat Transfer Measurements," AIAA 98–2501, Jan. 1998.
14. Crafton, J, Lachendro, N., Guille, M., Sullivan, J. P., "Application of Temperature and Pressure Sensitive Paint to an Obliquely Impinging Jet," AIAA–99–0387, Jan. 1999.
15. Ichimiya, K., "Heat Transfer Characteristics of an Annular Turbulent Impinging Jet with a Confined Wall Measured by Thermosensitive Liquid Crystal," Heat and Mass Transfer, published online Oct. 2002.
16. Maurel, S., and Solliec, C., "A Turbulent Plane Jet Impinging Nearby and Far from a Flat Plate," Exp. in Fluids, Vol. 31, pp. 687–696, 2001.
17. Tawfek, A.A., "Heat Transfer and Pressure Distributions of an Impinging Jet on a Flat Surface," Heat and Mass Trans., Vol. 32, pp. 49–54, 1996.

18. Huber, A.M. and Viskanta, R., "Effect of Jet-Jet Spacing on Convective Heat Transfer to Confined, Impinging Arrays of Axisymmetric Air Jets," Int. J. Heat Mass Trans., vol. 37, #18, pp. 2859–2869, 1994.
19. Huang, L. and El-Genk, M.S., "Heat Transfer of an Impinging Jet on a Flat Surface," Int. J. Heat Mass Trans., Vol. 37, #13, pp. 1915–1923, 1994.
20. Brown, J., Raghunathan, S., Watterson, J.K., Linton. A.J., and Riordon, D., "Heat Transfer Correlation for De-Icing Systems,"
21. Wright, W.B., "Users Manual for the NASA Lewis Ice Accretion Code LEWICE 2.2," NASA CR 209409, Jan. 1999.
22. Masiulaniec, K.C. and Wright, W.B., "User's Manual for the NASA Lewis Ice Accretion/Heat Transfer Prediction Code with Electrothermal Deicer Input", NASA CR–4530, 1994.
23. Wright, W.B., Al-Khalil, K.M., and Miller, D., "Validation of NASA Thermal Ice Protection Computer Codes: Part 2—Thermal De-Icing," AIAA–97–0050, Jan. 1997.
24. Al-Khalil, K.M., Miller, D. and Wright, W.B., "Validation of NASA Thermal Ice Protection Computer Codes: Part 3—Thermal Anti-Icing," AIAA–97–0051, Jan. 1997.
25. Lee, S., Addy, G and Broeren, A., “IRT Residual Icing Test on a Representative Piccolo Tube System,” Sept. 2003.

REPORT DOCUMENTATION PAGE

Form Approved
OMB No. 0704-0188

1. AGENCY USE ONLY (*Leave blank*)	2. REPORT DATE	3. REPORT TYPE AND DATES COVERED
	April 2004	Final Contractor Report

4. TITLE AND SUBTITLE

An Evaluation of Jet Impingement Heat Transfer Correlations for Piccolo Tube Application

5. FUNDING NUMBERS

WBS–22–728–41–17
NAG3–00145

6. AUTHOR(S)

William B. Wright

7. PERFORMING ORGANIZATION NAME(S) AND ADDRESS(ES)

QSS Group, Inc.
21000 Brookpark Road
Cleveland, Ohio 44135

8. PERFORMING ORGANIZATION REPORT NUMBER

E–14355

9. SPONSORING/MONITORING AGENCY NAME(S) AND ADDRESS(ES)

National Aeronautics and Space Administration
Washington, DC 20546–0001

10. SPONSORING/MONITORING AGENCY REPORT NUMBER

NASA CR—2004-212917
AIAA–2004–0062

11. SUPPLEMENTARY NOTES

Prepared for the 42nd Aerospace Sciences Meeting and Exhibit sponsored by the American Institute of Aeronautics and Astronautics, Reno, Nevada, January 5–8, 2004. Project Manager, Thomas Bond, Turbomachinery and Propulsion Systems Division, NASA Glenn Research Center, organization code 5840, 216–433–3900.

12a. DISTRIBUTION/AVAILABILITY STATEMENT

Unclassified - Unlimited
Subject Categories: 03 and 34 Distribution: Nonstandard

Available electronically at http://gltrs.grc.nasa.gov

This publication is available from the NASA Center for AeroSpace Information, 301–621–0390.

12b. DISTRIBUTION CODE

13. ABSTRACT ***(Maximum 200 words)***

Impinging jets have been used for a wide variety of applications where high rates of heat transfer are desired. This report will present a review of heat transfer correlations that have been published. The correlations were then added to the LEWICE software to evaluate the applicability of these correlations to a piccolo tube anti-icing system. The results of this analysis were then compared quantitatively to test results on a representative piccolo tube system.

14. SUBJECT TERMS

Conductive heat transfer; Thermodynamics

15. NUMBER OF PAGES

16

16. PRICE CODE

17. SECURITY CLASSIFICATION OF REPORT	18. SECURITY CLASSIFICATION OF THIS PAGE	19. SECURITY CLASSIFICATION OF ABSTRACT	20. LIMITATION OF ABSTRACT
Unclassified	Unclassified	Unclassified	